Available online at www.sciencedirect.com
SCIENCE DIRECT®
Journal of Contaminant Hydrology 85 (2006) 195–211
JOURNAL OF Contaminant Hydrology
www.elsevier.com/locate/jconhyd

Process-based reactive transport modeling of a permeable reactive barrier for the treatment of mine drainage

K.U. Mayer [a,*], S.G. Benner [b], D.W. Blowes [c]

[a] *Department of Earth and Ocean Sciences, University of British Columbia, 6339 Stores Road, Vancouver, British Columbia, Canada V6T 1Z4*
[b] *Department of Geosciences, Boise State University, Boise, Idaho 83725, USA*
[c] *University of Waterloo, Department of Earth Sciences, Waterloo, Ontario, Canada N2L 3G1*

Received 7 January 2005; received in revised form 31 January 2006; accepted 3 February 2006
Available online 22 March 2006

Abstract

Reactive transport modeling of a permeable reactive barrier for the treatment of mine drainage was used to integrate a comprehensive data set including pore water chemistry and solid phase data from several sampling events over a >3-year time period. The simulations consider the reduction of sulfate by the organic carbon-based treatment material and the removal of sulfate and iron by precipitation of reduced mineral phases including iron monosulfides and siderite. Additional parameters constraining the model include dissolved H_2S, alkalinity and pH, as well as a suite of solid phase S-fractions identified by extractions. Influences of spatial heterogeneity necessitated the use of a 2-dimensional modeling approach. Simulating observed seasonal fluctuations and long-term changes in barrier reactivity required the use of temperature dependent rate coefficients and a multimodal Monod-type rate expression accounting for the variable reactivity of different organic carbon fractions. Simulated dissolved concentrations of SO_4, Fe, H_2S, alkalinity and pH, as well as solid phase accumulations of reduced sulfur phases generally compare well to observed trends over 23 months. Spatial variations, seasonal fluctuations and the time-dependent decline in reactivity were also captured. The modeling results generally confirm, and further strengthen, the existing conceptual model for the site. Overall sulfate reduction and S-accumulation rates are constrained with confidence within a factor of 1.5.

Keywords: Reactive transport; Reaction kinetics; Sulfate reduction; Acid mine drainage; Reactive barrier; Remediation

* Corresponding author. Tel.: +1 604 822 1539; fax: +1 604 822 6088.
E-mail address: umayer@eos.ubc.ca (K.U. Mayer).

0169-7722/$ - see front matter © 2006 Elsevier B.V. All rights reserved.
doi:10.1016/j.jconhyd.2006.02.006

1. Introduction

In situ treatment in general, and permeable reactive barrier (PRB) technology in particular, have emerged as a viable approach for treating a suite of contaminants in the subsurface (e.g., Blowes et al., 2000; Tratnyek et al., 2003). A variety of mechanisms are employed within PRBs to improve water quality including abiotic or biotic contaminant conversion to benign reaction products, and/or contaminant attenuation by precipitation and/or adsorption (e.g., USEPA, 1998; Morrison et al., 2002). In all cases, assessing reactive barrier performance requires integrating complex, often kinetically limited, (bio)geochemical processes within a heterogeneous flow field.

Comprehensive, process-based reactive transport modeling is a versatile tool for evaluating and improving conceptual models of reactive barriers (e.g., Mayer et al., 2001; Yabusaki et al., 2001; Amos et al., 2004) or other complex systems that couple physical flow and biogeochemical processes (e.g., Postma and Appelo, 2000; Saiers et al., 2000; Guha et al., 2001; MacQuarrie et al., 2001; Gandhi et al., 2002; Steefel et al., 2003; Guha, 2004; Jurjovec et al., 2004). By simultaneously accounting for the physical transport processes and a suite of (bio)geochemical reactions, both kinetic and equilibrium controlled, while maintaining stoichiometric and system mass balance, a level of evaluation of complex systems can be achieved that would not otherwise be possible. Simulations are constrained by chemical interconnectivity; many dissolved species are involved in multiple reactions (e.g., Fe or H^+). This high level of connectivity typically implies that if the stoichiometry or rate of a simulated reaction is incorrect, the error propagates throughout the results making it impossible to reproduce the observed dataset. Despite the high level of control present in these types of simulations, the modeling results cannot be considered unique. However, this modeling approach can highlight areas of weakness or uncertainty within a conceptual model, illuminate potentially important processes that would otherwise be overlooked, and provide a quantitative assessment of complex system processes within a limited range of uncertainty.

This communication integrates data from a comprehensive field study (Benner et al., 1997, 1999, 2002; Herbert et al., 2000) and is the first attempt to assess the performance of a PRB for the treatment of mine drainage in a field setting using multicomponent reactive transport modeling. Our modeling efforts have focused on the quantitative evaluation of the conceptual model for the Nickel Rim permeable reactive barrier based on aqueous phase geochemical data (Benner et al., 2002) and solid phase sulfur geochemistry (Herbert et al., 2000). All references to field data are taken from these two publications unless otherwise noted. In addition, we have also attempted to expand our understanding of the spatial and seasonal variability in the barriers' performance over a 3.5-year time period. The simulations were conducted with the reactive transport code MIN3P (Mayer et al., 2002).

2. Site description: Nickel Rim permeable reactive barrier

The Nickel Rim reactive barrier installation provides a unique opportunity to apply process-based reactive transport modeling to a highly constrained field problem; the physical setting, coupled with the extensive monitoring network and sampling schedule provides well-defined boundary conditions and a comprehensive geochemical dataset not often found at a field site.

A plume of contaminated groundwater emanates from a tailings impoundment at the Nickel Rim mine site in Ontario, Canada, and migrates down a small alluvial aquifer before discharging to a nearby lake (Benner et al., 1997, Fig. 1). The groundwater contains elevated concentrations of Fe (3.6×10^{-3} to 3.6×10^{-2} mol l^{-1}/200–2000 mg l^{-1}) and SO_4 (1.0×10^{-2} to 4.2×10^{-2} mol l^{-1}/

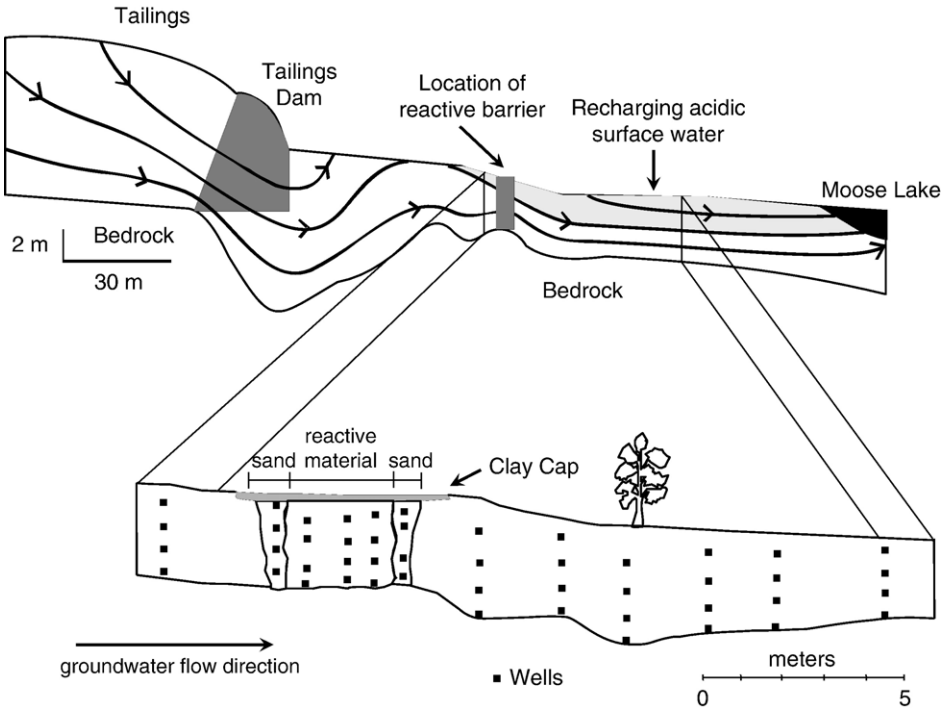

Fig. 1. Schematic description of Nickel Rim mine tailings site and investigation area for permeable reactive barrier study (modified from Benner et al., 1999).

1000–4000 mg l^{-1}) and is near neutral pH. However, upon discharge, the ferrous iron undergoes oxidation and precipitates as a Fe-oxide phase, producing acidity and driving the surface water pH <3. A permeable reactive barrier was installed in 1995 to treat the groundwater plume prior to discharge (Fig. 1). Detailed descriptions of the Nickel Rim site and the PRB can be found in Bain et al. (2000) and Benner et al. (1997, 1999, 2000, 2002). The reactive barrier, containing an organic carbon mixture, removes the acid generating Fe(II) from the pore water by promoting microbially mediated sulfate reduction and precipitation of Fe-bearing, sparingly soluble, sulfide mineral phase(s) and increasing alkalinity. The bedrock-bounded nature of the aquifer forms a well defined flow system with a known flux across the domain. The flow system is further constrained by chloride tracer data, which established the flow velocity through the barrier (16 m a^{-1}) with a relatively high level of accuracy and quantified zones of variable hydraulic conductivity within the barrier and aquifer (Fig. 3). The water chemistry monitoring network consisted of 12 well nests (4 sampling points each) aligned parallel to the direction of groundwater flow, up-gradient, within and down-gradient of the barrier. Sampling of this well array was conducted 9 times over a > 3-year period and comprehensive water analysis of these samples was conducted (Benner et al., 2002). Solid phase samples from within the barrier were collected 3 times over that period and temporal and spatial changes in solid phase speciation of sulfur and iron were quantified (Herbert et al., 2000), further constraining the mass balance for the system.

Significant spatial variations are observed in the amount of sulfate and iron removal within the barrier; lower sulfate concentrations are observed at the top and bottom compared to the mid-portion of the barrier (Fig. 2). This spatial variability has been attributed to differences in

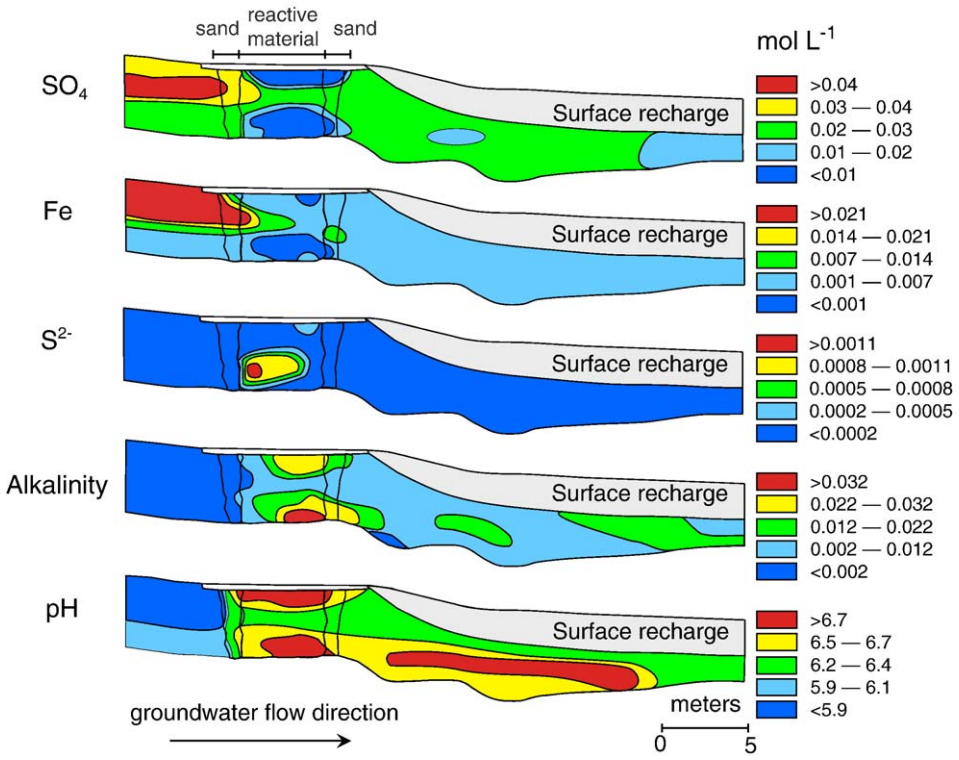

Fig. 2. Concentration contours of dissolved sulfate, iron, sulfide [mol l^{-1}], alkalinity [eq l^{-1}] and pH in the Nickel Rim PRB study area for July, 1997 (23 months of barrier operation, modified from Benner et al., 2002).

residence time. Higher flow velocities through the central portion of the barrier produce shorter residence times and less sulfate and iron removal for a given pore volume (Benner et al., 2002).

In addition, seasonal variations in SO_4 and Fe removal are observed. Typically sulfate concentrations measured within the PRB are lower during the summer months, while treatment appears to slow down during the winter. This variability is attributed to seasonal shifts in groundwater temperature; higher summer temperatures produce higher rates of microbially mediated sulfate reduction. Finally, the overall rate of sulfate reduction in the barrier declines over time and is attributed to consumption of the more reactive organic carbon fraction within the barrier (Benner et al., 2002).

3. From conceptual to numerical model

3.1. Physical framework

The reactive material was mixed with pea gravel to achieve a hydraulic conductivity that can accommodate the groundwater flow at the site. The porosity within the barrier and the aquifer were assumed $\phi = 0.4$ and 0.35, respectively. Benner et al. (2002) simulated the flow field at the site and expended considerable effort to ensure that groundwater velocities are representative of field conditions. The flow model calibration was based on chloride data collected from several multi-level piezometers over a 1-year period, data from borehole dilution tests conducted in the adjacent

aquifer, and previous regional scale flow modeling (Bain et al., 2000). Collectively, the field observations and numerical simulations provide a high level of constraint on the velocity field, which is a necessary requirement for making quantitative statements on treatment rates in a PRB. Flow and transport boundary conditions are also adopted from the flow and chloride tracer transport simulations by Benner et al. (2002) and are shown in Fig. 3. Groundwater passes though the barrier at an average flow velocity of 16 m a^{-1} but varies spatially with zones of lower conductivity at both the top and bottom of the barrier profile. The flow system also includes the recharge of acidic, untreated surface water on the down-gradient side of the reactive barrier (Fig. 3).

3.2. Chemical framework

The organic carbon within the barrier promotes microbially mediated sulfate reduction and metal sulfide precipitation, removing Fe and generating alkalinity (Benner et al., 1997). In this system, sulfate reduction can be expressed as:

$$CH_2O(s) + \frac{1}{2}SO_4^{2-} \Rightarrow HCO_3^- + \frac{1}{2}H_2S(aq) + H_2O \quad (1)$$

Due to the lack of information on reaction intermediates, the fermentation of organic carbon and the consumption of the fermentation products by sulfate reduction are described as an overall

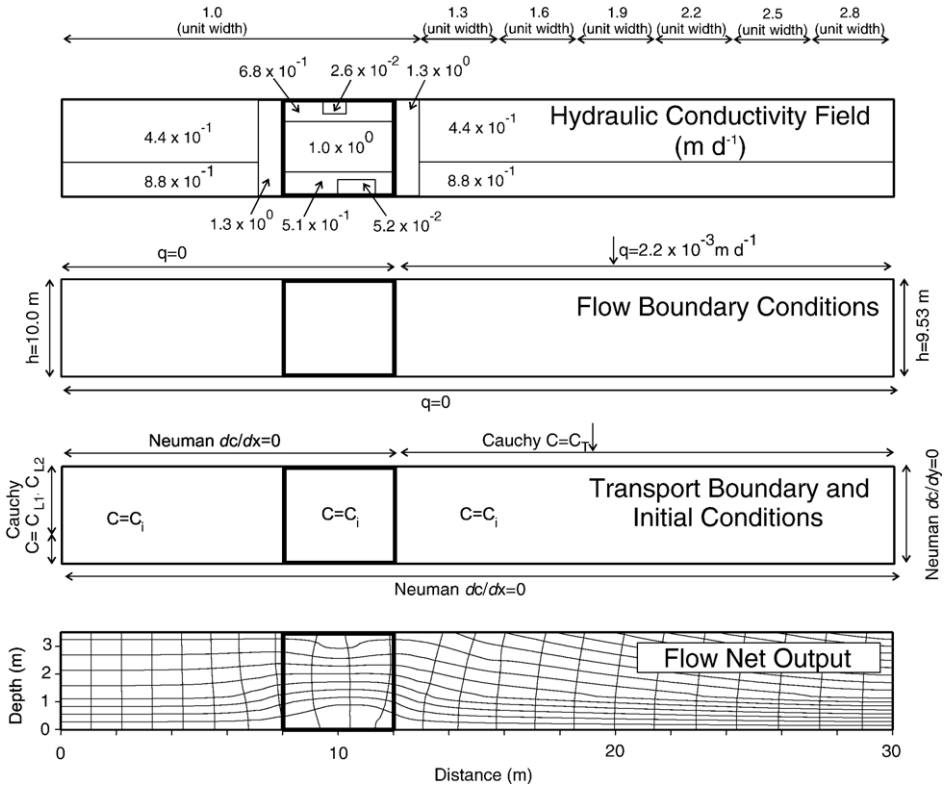

Fig. 3. Hydraulic conductivity field, flow boundary conditions, transport boundary and initial conditions, and flownet (modified from Benner et al., 2002).

reaction. A multi-modal Monod-type rate expression was used to simulate the observed long-term decline in barrier reactivity and rate dependence on sulfate concentration. This rate expression assumes that the most reactive organic carbon fraction is consumed first, causing the overall reactivity to decline asymptotically, an approach consistent with the widely accepted model of natural organic carbon as composed of a continuum of reactivities to oxidation (Westrich and Berner, 1984; Boudreau and Ruddick, 1991). The rate expression for sulfate reduction to sulfide is defined as:

$$R_{SO_4-H_2S} = -\sum_{i=1}^{N_{org}} k_{i,SO_4-H_2S}\left(\frac{[SO_4]}{K_{SO_4}+[SO_4]}\right) \tag{2}$$

where N_{org} is the number of organic carbon fractions with different reactivity, k_{i,SO_4-H_2S} is the effective rate coefficient for fraction i [mol dm^{-3} s^{-1}]. [SO_4] is the total concentration of dissolved sulfate [mol l^{-1}] and the half saturation constant (K_{SO_4}) equals 1.62×10^{-3} mol l^{-1} based on literature data (Boudreau and Westrich, 1984; Roychoudhury et al., 1998).

Acid volatile sulfides (AVS) have been identified as the dominant Fe-bearing sulfide mineral phases accumulating in the barrier (Herbert et al., 2000). The pore water is saturated to slightly supersaturated (SI=0–1.5) with respect to mackinawite and the AVS-sink has been described by mackinawite precipitation:

$$H_2S + Fe^{2+} \Rightarrow FeS(s) + 2H^+ \qquad \log K_{mac} = 4.65 \tag{3}$$

The formation of this phase has been simulated using a simple rate expression of the form (Steefel and van Cappellen, 1990; Steefel and MacQuarrie, 1996):

$$R_{min} = -k_{min}\left(1-\frac{IAP_{min}}{K_{min}}\right), \tag{4}$$

to honor thermodynamic constraints. In addition to the AVS fraction, the formation of a disulfide/S^0 fraction has been identified in the Nickel Rim PRB (Herbert et al., 2000). The exact reaction mechanism for the formation of the disulfide/S^0 is not known, but is likely due to incomplete sulfate reduction and/or the aging of mackinawite to disulfide phases. Alternatively, native sulfur may be formed by the reaction of H_2S with Fe-hydroxides; however, this pathway is less likely considering that Fe-hydroxides are not believed to be present in the original treatment mixture. This disulfide/sulfur sink is described by a second parallel sulfate reduction reaction that produces elemental sulfur (S^0):

$$CH_2O(s) + \frac{2}{3}SO_4^{2-} + \frac{1}{3}H^+ \Rightarrow HCO_3^- + \frac{2}{3}S^0(s) + \frac{2}{3}H_2O \tag{5}$$

The same type of rate expression used to describe the generation of sulfide (Eq. (2)) was applied to this reaction.

Organic carbon oxidation (reactions (1) and (5)) produces increased alkalinity and results in supersaturated conditions (SI=1–2) for siderite ($FeCO_3$), potentially promoting precipitation of this phase (Benner et al., 1999; Herbert et al., 2000). The accumulation of siderite was acknowledged as an additional sink for Fe in some portions of the barrier (Herbert et al., 2000) and can be expressed as:

$$Fe^{2+} + HCO_3^- \Leftrightarrow FeCO_3 + H^+ \qquad \log K_{sid} = 0.12 \tag{6}$$

Siderite precipitation may be enhanced by the dissolution of calcite, which was present in the original reactive mixture (1% by vol). This reaction is triggered by the slightly acidic nature of the water entering the barrier and is defined as:

$$CaCO_3 + H^+ \Leftrightarrow Ca^{2+} + HCO_3^- \qquad \log K_{cal} = 1.86 \tag{7}$$

In addition, gypsum dissolution and precipitation was allowed in the simulations. This reaction may be initiated due to the release of Ca from calcite dissolution into the high-SO_4 pore water:

$$CaSO_4 \cdot 2H_2O \Leftrightarrow Ca^{2+} + SO_4^{2-} + 2H_2O \qquad \log K_{gyp} = -4.58 \tag{8}$$

Dissolution precipitation reactions (6), (7) and (8) are quantified using the simple rate expression (Eq. (4)).

The formation of organically bound solid phase sulfur in significant concentrations was also identified (Herbert et al., 2000). Here, it is assumed that these compounds contain sulfur primarily in reduced form and the reaction is described as a first order irreversible process with respect to total dissolved sulfate concentrations.

In addition to the reactions described in this section, 21 equilibrium aqueous complexation reactions involving the components SO_4, S(-II), Fe(II), H^+, CO_3, and Ca were considered using equilibrium constants and activity correction parameters from the WATEQ4F database (USGS, 1991).

3.3. Boundary and initial conditions

Chemical stratification of the up-gradient aquifer (Fig. 2) necessitated a variable concentration distribution with higher Fe and SO_4 concentration influx in the top half of the left-hand boundary of the flow domain (Table 1). Over the simulation period, the observed depth integrated concentrations at the up-gradient end of the barrier ranged from 7–12 mmol l^{-1} for Fe and 24–36 mmol l^{-1} for SO_4 (Benner et al., 2002). Averaged concentrations were specified for the two depth zones (left-hand domain boundary), which yield depth-integrated concentrations of 11 mmol l^{-1} for Fe and 29 mmol l^{-1} for SO_4 (Table 2). Average conditions were also assumed for the surface water that does not pass through the barrier but infiltrates into the down-gradient aquifer (upper right domain boundary) and for the initial condition within the model domain (Table 1).

The up-gradient aquifer is assumed to contain pore water that is at quasi-equilibrium with the mineral phases present in the aquifer sediments and no reactions are allowed to proceed in this zone. Within the barrier, all of the reactions described in the conceptual model were allowed to

Table 1
Boundary and initial conditions for geochemical components, concentrations reported in [mol l^{-1}], data averaged from various sampling times (Benner et al., 1997, 1999, 2002)

	Upper left boundary	Lower left boundary	Top down-gradient boundary	Domain initial condition
Ca	1.0×10^{-2}	1.0×10^{-2}	1.2×10^{-2}	1.0×10^{-2}
Fe	2.2×10^{-2}	5.4×10^{-3}	1.2×10^{-2}	5.4×10^{-3}
SO_4	3.9×10^{-2}	2.3×10^{-2}	3.4×10^{-2}	2.3×10^{-2}
CO_3	8.3×10^{-4}	1.5×10^{-3}	7.9×10^{-4}	1.5×10^{-3}
pH	5.0	5.9	5.9	5.9

Table 2
Observed and simulated depth integrated concentrations of dissolved sulfate and iron [mmol l^{-1}], observed data from Benner et al. (2002)

	Observed		Simulated	
	Range	Average	Range	Average
Fe — up-gradient	7–12	10	N/A	11
Fe — down-gradient	0–6	3	0–4.3	2.2
Fe-removal	2–10	6	6–11	9
SO_4 — up-gradient	24–36	30	N/A	29
SO_4 — down-gradient	12–26	19	4–21	15
SO_4-removal	7–24	15	8–26	14

proceed. Within the down-gradient aquifer, precipitation reactions were permitted; however; reactions with aquifer mineral phases were not simulated.

In order to reproduce solid phase S-accumulation data by Herbert et al. (2000), organic carbon volume fractions were calculated based on an assumed organic carbon density of 0.6 g cm^{-3} and a dry bulk density of 0.2 g cm^{-3}, translating to a total organic carbon volume fraction of 0.333 cm^3 organic carbon cm^{-3} treatment material or 33.3 vol.% (Table 3). The remaining 26.7 vol.% are composed of calcite (1%) and pea gravel (25.7%), which is assumed non-reactive. The resulting total organic carbon volume fraction in the treatment mixture is slightly higher (organic carbon: pea gravel = 1.1:0.9) than the mixture that was installed at the site (1:1, Benner et al., 2002). However, there is some uncertainty associated with the composition and mixing ratio of the installed treatment material and organic carbon density values used in this simulation are within this uncertainty.

3.4. Influence of seasonal temperature variation

The dataset by Benner et al. (2002) facilitated the calculation of an activation energy value for sulfate reduction (E_a = 40 kJ mol^{-1}) that is used to express the dependence of the rate on

Table 3
Initial volume fractions and calibrated effective rate coefficients for organic carbon consumption and mineral dissolution–precipitation reactions

Reaction	$\varphi_{initial}$ [−]	Effective rate coefficient [mol dm^{-3} s^{-1}] [a]	Effective rate coefficient [mol dm^{-3} s^{-1}] [b]
CH_2O–H_2S (fast)	0.0007	1.0×10^{-9}	1.3×10^{-7}
CH_2O–S (fast)		3.0×10^{-10}	3.8×10^{-8}
CH_2O–H_2S (int.)	0.0013	1.0×10^{-9}	6.3×10^{-8}
CH_2O–S (int.)		3.0×10^{-10}	1.9×10^{-8}
CH_2O–H_2S (slow)	0.331	1.3×10^{-9}	4.2×10^{-9}
CH_2O–S (slow)		4.0×10^{-10}	1.3×10^{-9}
Calcite	0.01	5.0×10^{-10}	–
Mackinawite	–	5.0×10^{-11}	–
Siderite	–	5.0×10^{-12}	–
Gypsum	–	1.0×10^{-8}	–
Org S + other H_2S sinks	–	1.0×10^{-6}	–

[a] Normalized to bulk volume of treatment material.
[b] Normalized to volume of organic carbon fraction.

temperature. Groundwater temperature data were collected continuously for a year at four depths within the barrier (Benner et al., 2002). These data reveal the seasonal, sinusoidal, fluctuation in groundwater temperature of 7 °C at the base of the barrier and a 20 °C fluctuation at ground surface. The vertical temperature gradient also inverts biannually; groundwater at the bottom of the barrier is warmer in winter, the top of the barrier is warmer in summer. This field-collected data were used to construct a file containing the temperature field at every point within the barrier over time and depth and this file was then used as input to the Arrhenius equation for calculating the temperature dependence of sulfate reduction rate expression. These temperature values were also used to account for temperature dependence of equilibrium expressions (via the van't Hoff Equation). Thus the temperature dependence of the rates of sulfate reduction and all other kinetic and equilibrium reactions are simulated with respect to variations in both depth and time.

4. Model calibration

For the calibration of the model, we used both aqueous and solid phase data from various sampling events. In addition, the stoichiometric constraints of the individual reactions and the interconnectivity between the reactions were utilized in the calibration process. Overall sulfate reduction rates were calibrated to match the observed decline in SO_4 concentrations in the barrier based on pore water data from Benner et al. (2002). The relative distribution between the various solid phase sulfur accumulations (Herbert et al., 2000) were used to distinguish between the different pathways of sulfate removal, e.g., formation of sulfide (Eqs. (1) and (3)), elemental sulfur (Eq. (5)), precipitation as gypsum (Eq. (8)), and the formation of organically bound sulfur. The absolute values of solid phase sulfur accumulations are particularly valuable for model calibration, because they provide an integrated representation of treatment over the operational life of the barrier and allow an independent test if the calibrated aqueous phase rates and flow velocities, i.e., the SO_4-mass loading and removal within the barrier are described adequately.

Through the accumulation of mackinawite, iron removal by sulfide precipitation could be estimated (Eq. (3)). The remaining Fe(II) removed from solution was attributed to the formation of siderite (Eq. (6)). The rate coefficients for mackinawite and siderite formation were further constrained by the observed saturation conditions with respect to these phases. The calcite dissolution rate (Eq. (7)) was calibrated to approximate observed trends in pH and alkalinity yielding conditions close to saturation (Benner et al., 1999). Gypsum dissolution precipitation was treated as a quasi-equilibrium reaction (simulated SI < 0.01). Table 3 provides a summary of the calibrated reaction parameters.

Because the treatment efficiency of the PRB decreases over time, it was necessary to consider organic carbon fractions (Eq. (2)) of different reactivity. While the total organic carbon content is constrained by the composition of the installed material, the distribution of that carbon between the various fractions was calibrated to match the observed decline in sulfate reduction over time. Based on a series of preliminary simulations, the number of organic carbon fractions was set to $N_{org}=3$, representing fractions of fast, intermediate, and slow reactivity, in an attempt to approximate the reactive continuum representation of organic matter proposed by Boudreau and Ruddick (1991). For the given data set, we acknowledge that similar results may have been obtained using $N_{org}=2$. In addition to reporting rate coefficients normalized to the bulk volume of the treatment material, effective rate coefficients normalized to the organic carbon fraction are also provided to highlight the range of reactivity (Table 3).

5. Results and discussion

5.1. Comparison to field observations

The availability of both pore water (Benner et al., 2002) and solid phase data (Herbert et al., 2000) after 23 months of barrier operation is used to quantitatively compare model results to field data and evaluate how well the underlying conceptual model represents field observations.

Generally, the modeling results reproduce the observed concentration changes within the barrier well (compare Figs. 2 and 4). Simulated sulfate concentration decline to less than 2.2×10^{-2} mol l^{-1}, while maximum observed concentrations at the down-gradient end of the barrier range from $2–3\times10^{-2}$ mol l^{-1}. Simulated iron concentrations decrease to $< 6\times10^{-3}$ mol l^{-1}, while observed concentrations do not exceed 7×10^{-3} mol l^{-1}. Both simulated and observed sulfide concentrations only locally exceed values of 10^{-3} mol l^{-1} within the barrier. Simulated results indicate the presence of dissolved sulfide down-gradient of the barrier, which is not seen in the field data. This suggests that dissolved sulfide exiting the barrier is consumed by reactions with the aquifer minerals, a process which has not been simulated. Alkalinity ranges between 2×10^{-3} and 2×10^{-2} eq l^{-1} in average and reaches a maximum of approximately 3.5×10^{-2} eq l^{-1} in both simulated and observed data. Despite the large number of processes that affect pH in this system, the simulated pH range of 6.2–7 agrees well with the observed range of 6.2–6.7.

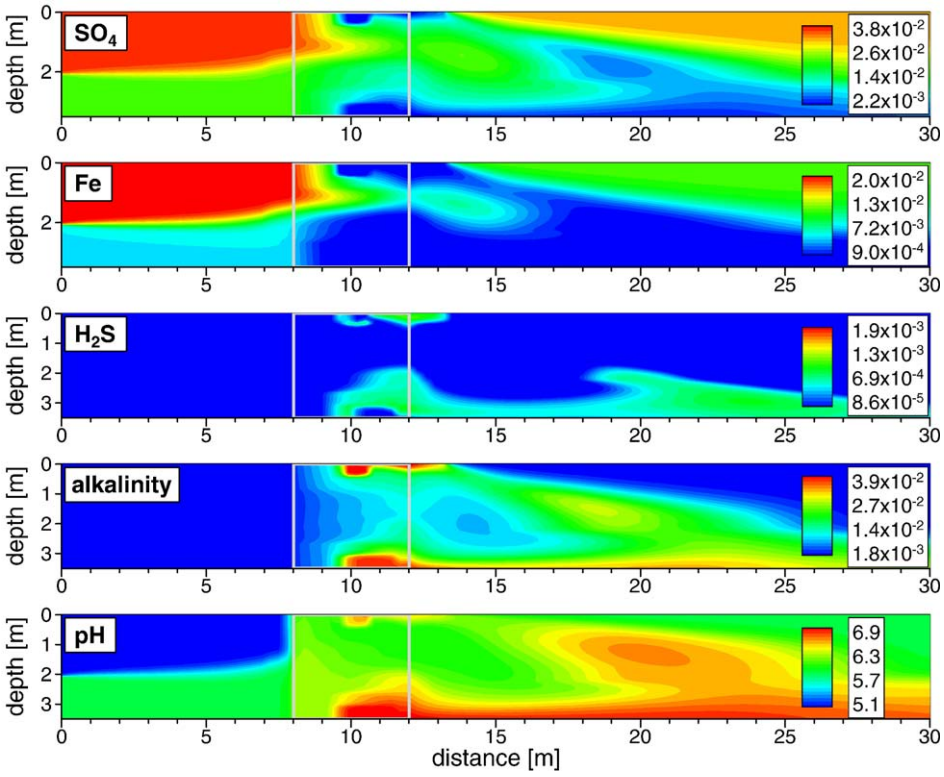

Fig. 4. Simulated concentration contours for SO_4, Fe, H_2S [mol l^{-1}], alkalinity [eq l^{-1}] and pH after 23 months of operation (July 1997).

The absolute accumulation of sulfur in solid phases was used to test the consistency of the model calibration. Precipitation of mackinawite, corresponding to the AVS fraction, represents by far the largest accumulation of mass within the barrier (Fig. 5), accounting for a total volume fraction of about 0.05 at the up-gradient side of the barrier. These results are consistent with Herbert et al. (2000), who estimated that approximately 75% of total reduced inorganic S (TRS) is present in the AVS fraction. Spatial averaging of the simulated results indicates that 60% of TRS exists in form of mackinawite (AVS). Maximum mackinawite accumulations contribute up to 72% to maximum simulated TRS (Table 4), which agrees well with previous results (Herbert et al., 2000). Maximum and average simulated absolute TRS accumulations (42 and 25 mol m^{-3}, respectively) also correspond well to observed buildup (43 and 28 mol m^{-3}, respectively, Table 4). It should be noted that simulated absolute S-accumulation values depend on the assumed organic carbon density. However, the ratio between the different S-fractions is not affected by the uncertainties regarding organic carbon density.

The simulations indicate that gypsum precipitation may only occur locally within the PRB (Fig. 5). Average observed inorganic solid phase SO_4 accumulations (Herbert et al., 2000) are significantly higher than simulated gypsum accumulations (6 and 0.6 mol m^{-3}, respectively, Table 4). This may be due to the fact that the measured inorganic SO_4 fraction does not only contain gypsum, but is also inclusive of pore water SO_4, and adsorbed SO_4 (Herbert et al., 2000). Alternatively, this trend may be attributed to the over-prediction of the organic-carbon bound S fraction (simulated versus observed: 11 versus 4 mol m^{-3}) by the model. Considering that the nature of the accumulation of organic S is not characterized, no further attempt was made to improve the simulation results with respect to organic S and gypsum formation.

Model results also suggest that siderite is precipitating within the reactive barrier, as was hypothesized by Benner et al. (1999). However, simulation results confirm that mackinawite

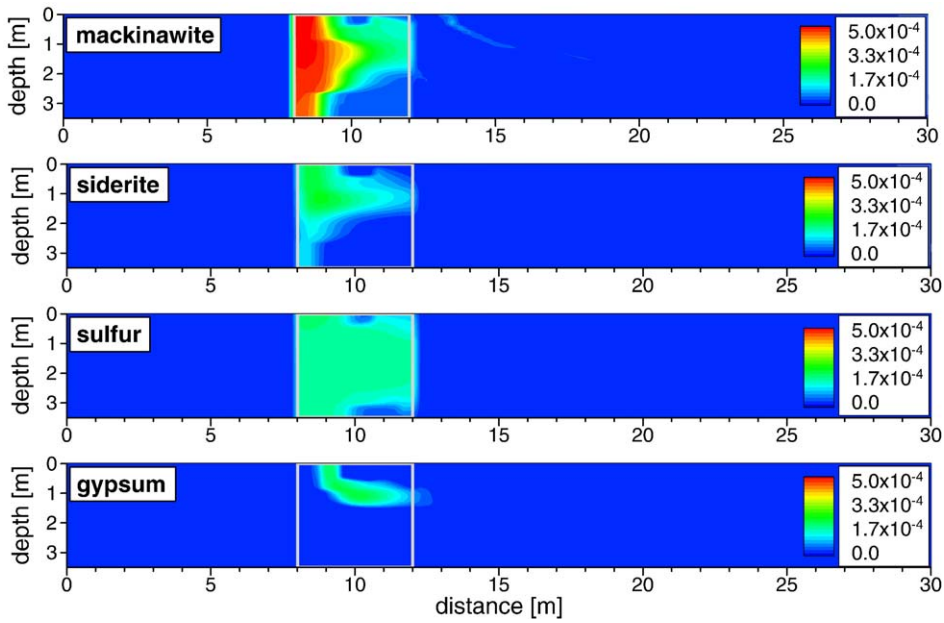

Fig. 5. Simulated concentration contours of mineral volume fractions [cm^3 mineral cm^{-3} treatment material] for mackinawite, siderite, sulfur, and gypsum after 23 months of operation (July 1997).

Table 4
Observed and simulated averaged S-accumulations in solid phase [mol m^{-3}] after 23 months of barrier operation

	Observed		Simulated	
	Maximum	Average	Maximum	Average
AVS[a] (Mackinawite)[b]	39	20	31	16
S^0/pyrite[a] (S^0)[b]	10	5	12	11
TRS[a] (Mackinawite + S^0)[b]	42	25	43	28
Org. S[a] (S-sink)[b]	8	4	27	11
SO_4–S[a] (Gypsum)[b]	21	6	3	0.6

Observed accumulations derived from the original data by Herbert et al. (2000) as reported by Daignault (2002) using a dry bulk density of 0.2 g organic carbon cm^{-3} treatment material.
[a] Measured parameter.
[b] Simulated mineral or mineral assemblage.

(AVS) is a far more significant sink for iron in this system (Fig. 5). Calcite dissolution is localized to the up-gradient end of the barrier; however, calcite is still abundant throughout the barrier after 23 months (not shown).

Overall, simulated results compare well with observed data, suggesting that the underlying concept adequately describes the geochemical processes within the PRB. These results are further supported by depth-integrated concentrations of Fe and SO_4 directly down-gradient of the PRB. Concentration averages over the first 37 months of barrier operation for Fe (2 mmol l^{-1}) and SO_4 (15 mmol l^{-1}) compare favorably with average depth-integrated concentrations calculated from observed data (Fe: 3 mmol l^{-1}, SO_4: 19 mmol l^{-1}) (Benner et al., 2002, Table 2). The simulations also indicate that the total mass accumulation is very small (< 0.2 vol.%), despite high SO_4 and Fe concentrations present in the untreated pore water, suggesting that there has been little change in porosity and permeability within the barrier as a result of these mass transfer reactions. The fact that hydraulic gradients remained relatively unchanged over the study period confirms these results (Benner, unpublished data).

5.2. Spatial variability

Zones of slower flow within the simulations exhibit markedly lower concentrations of SO_4 and Fe and elevated alkalinity and pH (Fig. 4), consistent with trends observed in the actual barrier (Fig. 2). Interestingly, the simulations highlight the fact that lower concentrations do not necessarily translate into elevated rates of solid phase accumulation (Fig. 5); higher SO_4 flux rates through the central portion of the barrier result in greater sulfide accumulation, while sulfate concentrations remain elevated (Figs. 4 and 5). Conversely, in slower flowing zones at the top and bottom of the barrier, where SO_4 concentrations are low, much less total sulfide accumulation is observed (Fig. 5). These trends confirm the importance of variations in hydraulic conductivity in controlling the degree of treatment within the barrier and illustrate how hydraulic conductivity variations translate into decreases in sulfate reduction efficiency. In the zone of low hydraulic conductivity at the top and bottom of the barrier, where sulfate transport limits the rates, simulated sulfate reduction rates after 23 months are as low as 5×10^{-13} mol dm^{-3} s^{-1} while in the central

portion of the barrier, where sulfate reduction is not transport limited reduction rates range from 3×10^{-10} to 1×10^{-9} mol dm^{-3} s^{-1}.

The model results also indicate greater accumulation of sulfides as well as other Fe-minerals (such as siderite) at the front of the barrier, where thermodynamic gradients are highest (Fig. 5). These results are consistent with solid phase data from the barrier (Herbert et al., 2000), and confirm that the rate of sulfate reduction was at least historically highest at the up-gradient end of the barrier, a result captured by the SO_4-dependent term in the sulfate reduction rate expression.

5.3. Seasonal variations

The influence of changing temperatures on sulfate reduction is complex and the modeling results provide a view of this process that is not clearly illustrated in the field-collected data. Time series of sulfate concentration contours from the simulations illustrate the impact of changing temperature on the degree of sulfate reduction (Fig. 6). Seasonal variations in the rate of sulfate reduction within the barrier (Fig. 7) translate into spatial heterogeneity in sulfate concentrations within and down-gradient of the barrier (Fig. 6).

Rates of sulfate reduction are generally higher in the summer months, but also show discrete temperature-dependent changes versus depth and capture the time-delayed response of subsurface temperatures and rates to seasonal temperature variations at the ground surface (Fig. 7). As a result, pore water that passed through the barrier during the winter months contains elevated SO_4 concentrations, while pore water that migrated through the barrier during the summer months contains lower SO_4 concentrations (Fig. 6). These changes remain visible in the pore water that has left the PRB. Similar trends are also present in the simulated cross sections for Fe, alkalinity, and pH (not shown).

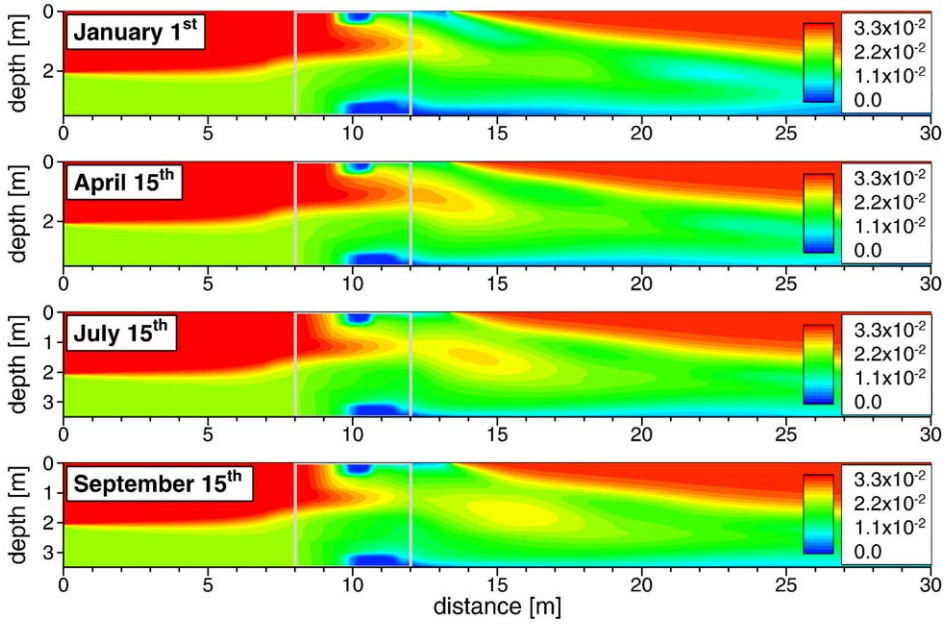

Fig. 6. Seasonal variations of sulfate concentrations [mol l^{-1}] for 1998 (29–41 months of barrier operation).

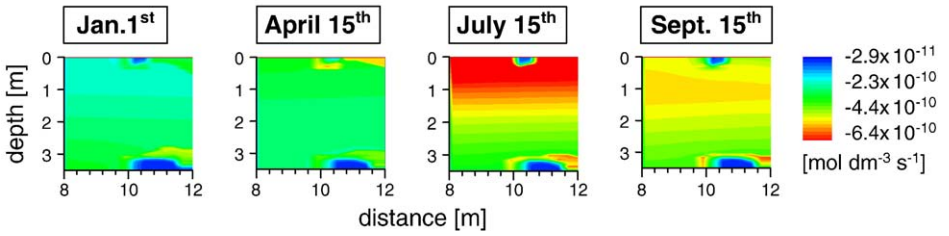

Fig. 7. Simulated contours of organic carbon consumption rates by sulfate reduction [mol dm^{-3} s^{-1}] for 1998 (29–41 months of barrier operation).

Limitations in the field-collected dataset, including temporal data restricted to biannual sampling, as well as variations in the chemical composition of the untreated groundwater, preclude the definitive expression of these seasonal trends in cross-sectional contour plots and prevent direct comparison to the simulated results. However, calculated rates based on pore water geochemistry data from several sampling events (Benner et al., 2002) compare well to simulated seasonal changes of sulfate reduction rates averaged over the entire cross section of the PRB (Fig. 8). In addition, observed ranges of depth-integrated iron and sulfate removal varied from 2–10 mmol l^{-1} and 7–24 mmol l^{-1}, respectively, which is in fairly good agreement with simulated removal (Fe: 6–11 mmol l^{-1}, SO_4: 8–26 mmol l^{-1}) (Table 2).

5.4. Long-term trends

Both observed, as well as simulated sulfate reduction rates show a decrease over time (Fig. 8), and compare well with the long-term trend derived by Benner et al. (2002). This has previously been attributed to the presence of various organic carbon fractions (Benner et al., 2002) and is here described using the multimodal Monod expression defined by Eq. (2). Using this rather simplistic model, the simulated sulfate reduction rates show zones of increased sulfate reduction, which cannot be attributed to seasonal changes (Fig. 7). These zones are typically located near low permeability lenses or can be found in down-gradient areas of the PRB that show lower sulfate concentrations, but are not entirely devoid of sulfate (compare to Fig. 6). A further examination of the simulation results shows that the "intermediate" organic carbon fraction (Table 3) is still present in these zones and illustrates the complex interactions between barrier heterogeneity, sulfate mass loading into a particular area, and treatment material consumption. After 23 months of barrier operation only 13% of the "intermediate" organic carbon fraction

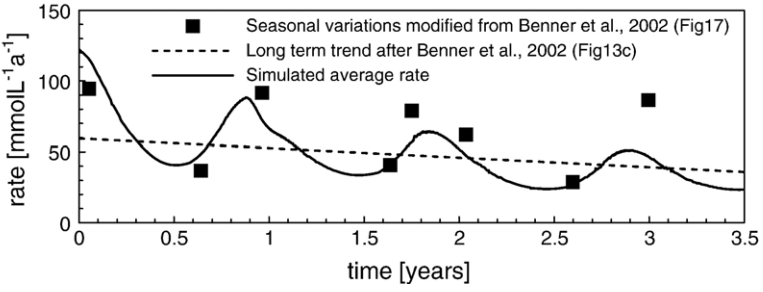

Fig. 8. Seasonal variations and long-term trend of average sulfate reduction rates.

remains in the PRB. The "fast" fraction is almost entirely consumed (only 4% remain in low flow zones, which are inaccessible to sulfate), while the "slow" fraction is almost untouched (> 99% remain).

It should be noted that treatment material may also be consumed by fermentation reactions and methanogenesis, which was not simulated here. It is also clear that this model does not fully describe the complexity of the organic carbon assemblage; however, the general trend of overall reactivity decline is well described. It can also be expected that the remaining "slow" fraction will have to be further subdivided to predict barrier performance beyond the simulated 3.5 years. This makes the quantitative prediction of the long-term barrier performance difficult and we therefore refrain from extrapolating the model results beyond the time frame of the available data set. However, it is likely that future decline in barrier reactivity will be less significant assuming that the reactivity decrease will follow a similar trend to that observed for organic carbon contained in marine sediments (Boudreau and Ruddick, 1991).

The simulation results can also be compared to observed solid phase accumulations within the PRB, which are available at 3, 14 and 23 months (Herbert et al., 2000) (Table 4 and Fig. 9). As previously mentioned, direct comparison of the simulated and observed solid phase accumulations is hampered by uncertainty regarding the in situ density of the organic carbon and also barrier porosity. If organic carbon densities would be lower or if the effective porosity would be higher, the simulations would tend to overestimate solid phase sulfur accumulations based on calibrated aqueous sulfate reduction rates. In acknowledgement of this uncertainty, a shaded zone has been added to Fig. 9 for a range of 0.15 to 0.25 g cm^{-3} for the organic carbon dry bulk density.

Observed solid phase accumulations of TRS (sum of mackinawite and S^0 in the model) and corresponding rates emphasize the initial rapid buildup of reduced sulfur phases. Simulated TRS accumulations plot below the observed accumulations early during barrier operation. However,

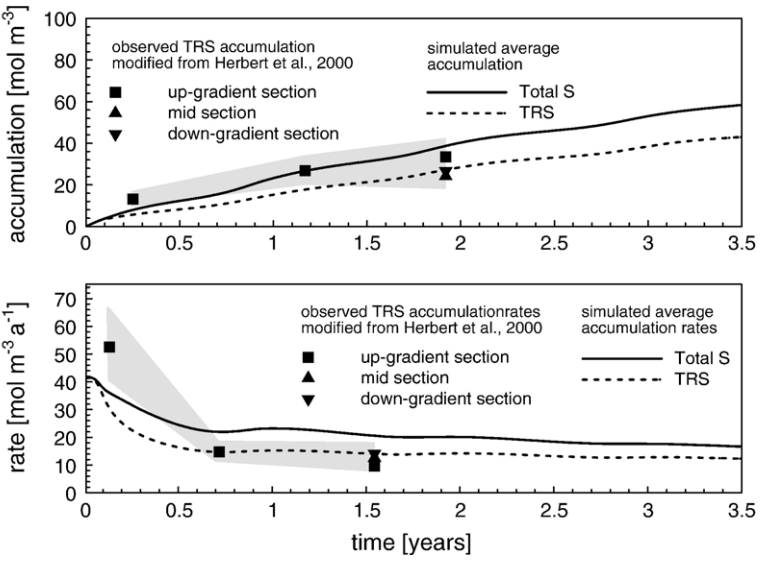

Fig. 9. Total sulfur and TRS (AVS + S^0/pyrite) accumulation and accumulation rates in solid phase (data from Herbert et al., 2000). Observed accumulations derived from the original data by Herbert et al. (2000) as reported by Daignault (2002) using a dry bulk density of 0.2 g organic carbon cm^{-3} treatment material, grey shaded area corresponds to range of dry bulk densities of 0.15–0.25 g cm^{-3}.

the early observed data are representative only for the up-gradient portion of the PRB, which is characterized by higher reduced sulfur accumulations (Fig. 5), while the simulated data represent an average over the entire PRB. Seasonal changes in simulated sulfur accumulation rates appear to be somewhat dampened in comparison to simulated aqueous removal rates. This may be due in part to kinetic limitations of sulfide formation, but is also an artifact of back calculating the rates from simulated accumulations. Overall, the simulation is successful in matching the sulfide accumulation after 23 months of barrier operation.

Both observed data and simulation results suggest that treatment is initially rapid and that the barrier may "over perform" at early time; however, this effect is rather short lived (3–6 months). Attempting to optimize the treatment material by excluding "too reactive" portions may therefore not be of significant benefit. On the other hand, results indicate clearly that the adaptation period for sulfate reducing bacteria is short and can be neglected in this system, i.e., there is essentially no lag time until treatment is initiated, and that the system should be designed based on long-term and not on short-term rates to remain operational for a reasonable period of time.

6. Conclusions

Reactive transport modeling was used to integrate a comprehensive data set composed of pore water and solid phase data from a permeable reactive barrier. The model calibration was constrained by the reaction stoichiometries of the individual reactions and the interconnectivity between the reactions, Overall good agreement between simulated sulfate reduction rates, iron removal, secondary geochemical parameters such as alkalinity and pH, and solid phase accumulations suggests that the existing conceptual model is a valid representation of processes that are taking place in the field. The availability of a detailed data set allowed the investigation of seasonal changes, spatial variations, and decline of sulfate reduction rates with increasing age of the barrier. The simulations could also be used to highlight potential discrepancies in aqueous sulfate reduction rates and solid phase sulfur accumulations, which can most likely be explained by uncertainties of in situ parameters such as organic carbon density and effective porosity within the PRB. Nevertheless, by integrating pore water and solid phase data using the current reactive transport modeling approach, it can be stated with reasonable certainty that the simulated overall rate of sulfate reduction is within a factor of 1.5 of the field rates.

Acknowledgements

Financial support for this research was provided by Falconbridge Ltd., CANMET, the Canadian Water Network (CWN), and the Natural Sciences and Engineering Research Council of Canada (NSERC).

References

Amos, R.T., Mayer, K.U., Blowes, D.W., Ptacek, C.J., 2004. Reactive transport modeling of column experiments for the remediation of acid mine drainage. Env. Sci. Technol. 38, 3131–3138.

Bain, J.G., Blowes, D.W., Robertson, W.D., Frind, E.O., 2000. Modelling of sulfide oxidation with reactive transport at a mine drainage site. J. Contam. Hydrol. 41, 23–47.

Benner, S.G., Blowes, D.W., Ptacek, C.J., 1997. Full-scale porous reactive wall for the prevention of acid mine drainage. Groundwater Monitoring and Remediation 17, 99–107.

Benner, S.G., Herbert Jr., R.B., Blowes, D.W., Ptacek, C.J., Gould, D., 1999. Geochemistry and microbiology of a permeable reactive barrier for acid mine drainage. Environ. Sci. Technol. 33, 2793–2799.

Benner, S.G., Gould, D., Blowes, D.W., 2000. Microbial populations associated with the generation and treatment of acid mine drainage. Chem. Geol. 169, 435–448.

Benner, S.G., Blowes, D.W., Ptacek, C.J., Mayer, K.U., 2002. Rates of sulfate reduction and metal sulfide precipitation in a permeable reactive barrier. Appl. Geochem. 17, 301–320.

Blowes, D.W., Ptacek, C.J., Benner, S.G., McRae, C.W.T., Bennett, T.A., Puls, R.W., 2000. Treatment of inorganic contaminants using permeable reactive barriers. J. Contam. Hydrol. 45, 123–137.

Boudreau, B.P., Ruddick, B.R., 1991. On a continuum representation of organic matter diagenesis. Am. J. Sci. 291, 507–538.

Boudreau, B.P., Westrich, J.T., 1984. The dependence of bacterial sulfate reduction on sulfate concentration in marine sediments. Geochim. Cosmochim. Acta 48, 2502–2516.

Daignault, E.C.M., 2002. The solid phase sulphur speciation of metal sulphides in a permeable reactive barrier, Nickel Rim mine, Sudbury, Ontario, B.Sc. thesis, University of Waterloo, Waterloo, ON.

Gandhi, R.K., Hopkins, G.D., Goltz, M.N., Gorelick, S.M., McCarty, P.L., 2002. Full-scale demonstration of in situ cometabolic biodegradation of trichloroethylene in groundwater: 2. Comprehensive analysis of field data using reactive transport modeling. Water Resour. Res. 38, 1040. doi:10.1029/2001WR000380.

Guha, H., 2004. Biogeochemical influence on transport of chromium in manganese sediments: experimental and modeling approaches. J. Contam. Hydrol. 70, 1–36.

Guha, H., Saiers, J.E., Brooks, S., Jardine, P., Jayachandran, K., 2001. Chromium transport, oxidation, and adsorption on manganese-coated sand. J. Contam. Hydrol. 49, 311–334.

Herbert Jr., R.B., Benner, S.G., Blowes, D.W., 2000. Solid phase iron-sulfur geochemistry of a reactive barrier for treatment of mine drainage. Appl. Geochem. 15, 1331–1343.

Jurjovec, J., Blowes, D.W., Ptacek, C.J., Mayer, K.U., 2004. Multicomponent reactive transport modelling of acid neutralization reactions in mill tailings. Water Resour. Res. 40, W11202. doi:10.1029/2003WR002233.

MacQuarrie, K.T.B., Sudicky, E.A., Robertson, W.D., 2001. Multicomponent simulation of wastewater-derived nitrogen and carbon in shallow unconfined aquifers: II. Model application to a field site. J. Contam. Hydrol. 47, 85–104.

Mayer, K.U., Blowes, D.W., Frind, E.O., 2001. Reactive transport modeling of an in situ reactive barrier for the treatment of hexavalent chromium and trichloroethylene in groundwater. Water Resour. Res. 37, 3091–3104.

Mayer, K.U., Frind, E.O., Blowes, D.W., 2002. Multicomponent reactive transport modeling in variably saturated porous media using a generalized formulation for kinetically controlled reactions. Water Resour. Res. 38. doi:10.1029/2001WR000862.

Morrison, S.J., Naftz, D.L., Davis, J.A., Fuller, C.C., 2002. Introduction to groundwater remediation of metals, radionuclides, and nutrients with permeable reactive barriers. In: Naftz, D.L., Morrison, S.J., Davis, J.A., Fuller, C.C. (Eds.), Handbook of Groundwater Remediation Using Permeable Reactive Barriers. Academic Press, San Diego, CA, p. 539. Chap. 1.

Postma, D., Appelo, C.A.J., 2000. Reduction of Mn-oxides by ferrous iron in a flow system: column experiment and reactive transport modeling. Geochim. Cosmochim. Acta 64, 1237–1247.

Roychoudhury, A.N., Viollier, E., van Cappellen, P., 1998. A plug flow-through reactor for studying biogeochemical reactions in undisturbed aquatic sediments. Appl. Geochem. 13, 269–280.

Saiers, J.E., Guha, H., Jardine, P., Brooks, S., 2000. Development and evaluation of a mathematical model for the transport and oxidation–reduction of CoEDTA. Water Resour. Res. 36, 3151–3165.

Steefel, C.I., MacQuarrie, K.T.M., 1996. In: Lichtner, P.C., Steefel, C.I., Oelkers, E.H. (Eds.), Reactive transport in porous media. Reviews of Mineralogy, vol. 34. Mineralogical Society of America, Warrendale, PA. Chap. 2.

Steefel, C.I., van Cappellen, P., 1990. Geochim., Cosmochim., Acta 54, 2657–2677.

Steefel, C.I., Carroll, S., Zhao, P., Roberts, S., 2003. Cesium migration in Hanford sediment: a multisite cation exchange model based on laboratory transport experiments. J. Contam. Hydrol. 67, 219–246.

Tratnyek, P.G., Scherer, M.M., Johnson, T.J., Matheson, L.J., 2003. Permeable reactive barriers of iron and other zero-valent metals. In: Tarr, M.A. (Ed.), Chemical Degradation Methods for Wastes and Pollutants: Environmental and Industrial Applications. Marcel Dekker, New York, pp. 371–421.

USEPA, 1998. Permeable reactive barrier technologies for contaminant remediation, EPA/600/R-98/125.

USGS, 1991. User's Manual for WATEQ4F, with revised thermodynamic database and test cases for calculating speciation of major, trace and redox elements in natural waters, Open-File Report 91–183, 189 pp. plus diskette.

Westrich, J.T., Berner, R.A., 1984. The role of sedimentary organic matter in bacterial sulfate reduction: the G model tested. Limnol. Oceanogr. 29, 236–249.

Yabusaki, S., Cantrell, K., Sass, B., Steefel, C., 2001. Multicomponent reactive transport in an in situ zero-valent iron cell. Environ. Sci. Technol. 35, 1493–1503.